Nanosized Aspirin-Arg-Gly-Asp-Val: Delivery of Aspirin to Thrombus by the Target Carrier Arg-Gly-Asp-Val Tetrapeptide

Shaoming Jin,[†,⊥] Yaonan Wang,[‡,⊥] Haimei Zhu,[†] Yuji Wang,[†] Shurui Zhao,[‡] Ming Zhao,[†,§,*] Jiawang Liu,[†] Jianhui Wu,[†] Wen Gao,[†] and Shiqi Peng[†,*]

[†]College of Pharmaceutical Sciences, Capital Medical University, Beijing 100069, People's Republic of China, [‡]Medical Experiment and Test Center, Capital Medical University, Beijing 100069, People's Republic of China, and [§]Faculty of Biomedical Science and Environmental Biology, Kaohsiung Medical University, Kaohsiung, Taiwan. [⊥]S. Jin and Y. Wang contributed equally to this work.

ABSTRACT Resistance and nonresponse to aspirin dramatically decreases its therapeutic efficacy. To overcome this issue, a small-molecule thrombus-targeting drug delivery system, aspirin-Arg-Gly-Asp-Val (A-RGDV), is developed by covalently linking Arg-Gly-Asp-Val tetrapeptide with aspirin. The 2D ROESY NMR and ESI-MS spectra support a molecular model of an A-RGDV tetramer. Transmission electron microscopy images suggest that the tetramer spontaneously assembles to nanoparticles (ranging from 5 to 50 nm in diameter) in water. Scanning electron microscopy images and atomic force microscopy images indicate that the smaller nanoparticles of A-RGDV further assemble to bigger particles that are stable in rat blood. The delivery investigation implies that in rat blood A-RGDV is able to keep its molecular integrity, while in a thrombus it releases aspirin. The *in vitro* antiplatelet aggregation assay suggests that A-RGDV selectively inhibits arachidonic acid induced platelet aggregation. The mechanisms of action probably include releasing aspirin, modifying cyclic oxidase, and decreasing the expression of GPIIb/IIIa. The *in vivo* assay demonstrates that the effective antithrombotic dose of A-RGDV is 16700-fold lower than the nonresponsive dose of aspirin.

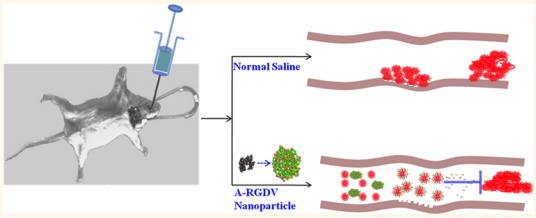

KEYWORDS: aspirin · RGDV · nanomedicine · GPIIb/IIIa · cyclooxygenase · thrombus

Aspirin has enjoyed its medicinal popularity for over 110 years. The therapeutic usage of aspirin in diverse indications, such as acute inflammation and pain,[1,2] cardiovascular diseases,[3−7] stroke,[8,9] pregnancy complications,[10,11] cancer,[12−14] diabetes,[15−18] and Alzheimer's disease,[19,20] reflects its colorful achievements. However, clinical trials have also exposed the limitations of aspirin therapy. The major problem is implicated in the resistance or nonresponse to aspirin. Aspirin resistance and nonresponse are defined as the incomplete inhibition of platelet function of the patients treated with aspirin, even though the patients with a specific disease receive a clinically effective dosage. This phenomenon severely decreases the therapeutic efficacy of aspirin in the treatment of various diseases including type 2 diabetes,[15,21] asthma,[22,23] cardiovascular disease,[24,25] stroke,[26] coronary artery disease,[27,28] and pediatric cardiac surgery.[29] A series of efforts have been made in order to overcome the clinical shortcomings of aspirin. For example, to increase the platelet sensitivity of diabetes mellitus patients, excellent near-normal metabolic control was clarified and the dosing schedules of aspirin were altered;[30] to increase the platelet sensitivity of cardiovascular patients having elevated plasma cholesterol, aspirin was combined with an inhibitor of lipid peroxidation;[31] to increase the platelet sensitivity of cardiovascular patients at risk for secondary atherothrombosis, aspirin was combined with a statin;[32] to increase the sensitivity of colon cancer, aspirin was covalently linked to nontoxic well-defined 3-hydroxybutanoic acid oligomers;[33] to avoid aspirin intolerance, patients were recommended to use alternative drugs;[34] and to enhance the safety of oral aspirin challenge in patients with aspirin-exacerbated respiratory disease, pretreatment with leukotriene-modified drugs

* Address correspondence to shiqipeng@163.com or sqpeng@bjmu.edu.cn; mingzhao@bjmu.edu.cn.

Received for review April 30, 2013 and accepted August 11, 2013.

Published online August 12, 2013
10.1021/nn402171v

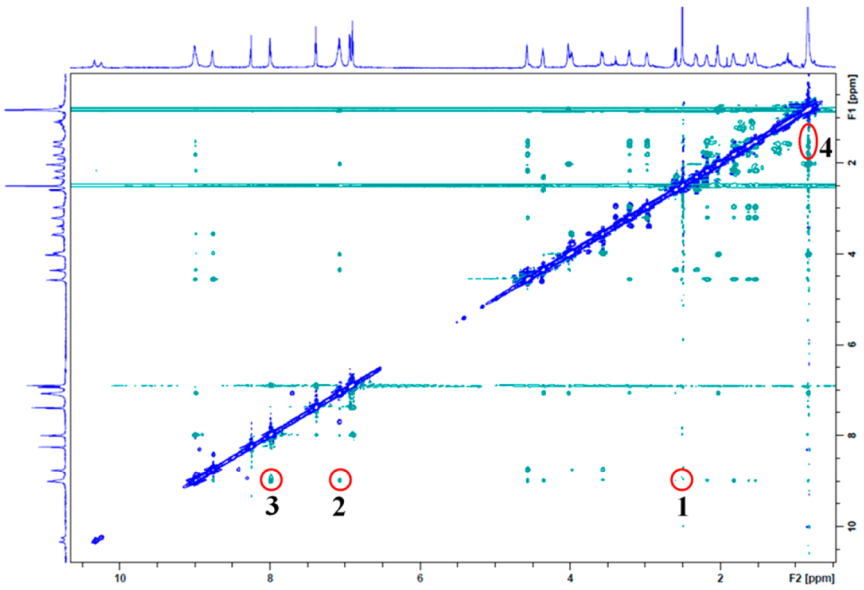

Figure 1. ROESY 2D NMR spectrum and the four cross-peaks. Cross-peak 1 defines the conformation of A-RGDV, while cross-peaks 2−4 define the intermolecular aggregation of A-RGDV.

was recommended.[35] In spite of some achievements made by these efforts, resistance and nonresponse remains the major obstacle for the utility of aspirin in the treatment of various diseases including cardiovascular diseases.

The RGD sequence is the motif of integrins recognizing collagen, fibronectin, vitronectin, laminin, members of the immunoglobulin superfamily, and the plasma proteins. The interaction of integrins with the RGD sequence has been widely used to prepare drug delivery systems. The efforts focusing on the adhering property of the RGD sequence toward integrins resulted in the development of biomaterials, such as the amphiphilic block copolymer PCLAePEGePCLA,[36] hydroxyapatite biomaterials,[37] collagen tubes,[38] covalent conjugates containing a substrate that promotes cell adhesion and cell spreading,[39] and mussel adhesive proteins.[40] The efforts focusing on the targeting property of the RGD sequence toward GPIIb/IIIa of activated platelets led to the development of antithrombotic agents, such as the RGD peptides covalently attached to liposomes,[41,42] modified RGD sequences,[43] and the epitope of apolipoprotein A.[44]

Aiming at avoiding resistance and nonresponse to aspirin,[22,23,45,46] this study tested a hypothesis that RGDV covalently modified aspirin, aspirin-Arg-Gly-Asp-Val (A-RGDV), should be stable in the circulation, release aspirin in thrombi, and inhibit the formation of thrombi.

RESULTS AND DISCUSSION

ROESY 2D NMR Spectrum Identifying the Intermolecular and Intramolecular Interactions of A-RGDV. To know if intermolecular and intramolecular interactions driving A-RGDV form nanoparticles, the ROESY 2D NMR spectrum was measured at 800 MHz in deuterated DMSO and is shown in Figure 1, in which four cross-peaks are labeled with red circles. Cross-peak 1 is the interaction between the acetyl-CH_3 of aspirin and the guanidine-H of the arginine residue. This indicates that the guanidine-H of the arginine residue and the O of the acetyl group of the aspirin residue likely form a hydrogen bond, thereby the aspirin-arginine moiety of A-RGDV takes a ring-like conformation (see Figure 5). Cross-peak 2 is for the H of the amide of the aspartic acid residue and the H of the guanidino of the arginine residue, cross-peak 3 is for the *o*-H of phenyl of aspirin and the H of the amide of the aspartic acid residue, and cross-peak 4 is for the H of the methyl groups of the valine residue and the H of the β- and γ-CH_2 of the side chain of the arginine residue. These cross-peaks demonstrate that the distances between the phenyl of one molecule and the peptide chain of another molecule, as well as the distance between the peptide chain of one molecule and the peptide chain of another molecule, are <4 Å. The moieties being in close vicinity reflect the stereochemical relationship of the molecules of A-RGDV and suggest that intermolecular interactions should be responsible for A-RGDV forming a molecular aggregate.

ESI-MS Spectrum Supporting A-RGDV Existing as Tetramers. The intermolecular interactions were further evidenced with an ESI-MS spectrum of A-RGDV in water (Figure 2). The mass of 2261.45306 of the ion peak (in the inset) equals the mass of four molecules of A-RGDV (565.11528 × 4 + H) losing acetyl groups. This means that in water A-RGDV exists as tetramers. The ESI-MS spectrum also gives the ion peak of 1697.73621, which equals the mass of a trimer of A-RGDV (565.11528 × 3 + H) losing acetyl groups, the ion peak of 1131.45904, which

equals the mass of a dimer of A-RGDV (565.11528 × 2 + H) losing acetyl groups, and the ion peak of 566.11528, which equals the mass of a monomer of A-RGDV (565.11528 + H) losing an acetyl group. Of the ion peaks the dimer has the highest ion peak. These ion peaks demonstrate that in the ESI-MS condition the tetramer could be gradually split into trimer, dimer, and monomer.

TEM and SEM Images of A-RGDV. The nanostructures of A-RGDV in an aqueous solution of pH 7.2 and in the solid state were observed with transmission electron microscopy (TEM) and scanning electron microscopy (SEM), respectively. In aqueous solution at pH 7.2 A-RGDV formed nanoparticles of 5−175 nm in diameter, and the diameter of more than 90% of nanoparticles is less than 50 nm (Figure 3A). This is the desirable diameter for nanoparticles to escape phagocytosis by macrophages, benefiting the delivery of A-RGDV in the circulation.[47] The solid form of A-RGDV is an egg shaped particle, 2−14 μm in length. On the surface of the egg labeled with a pink line some small particles could be found, which implies that the eggs are built of small particles (Figure 3B). SEM images allow us to propose that in aqueous solution the eggs can disperse and convert to nanoparticles having the mentioned diameter.

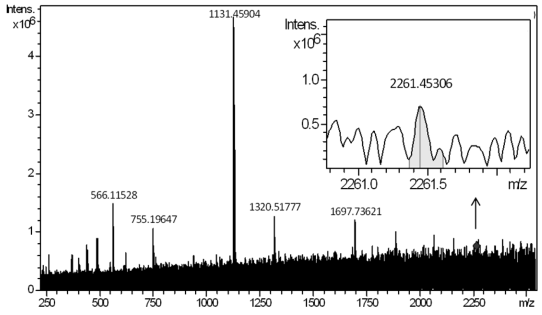

Figure 2. ESI-MS spectrum of A-RGDV. The ion peak of the A-RGDV tetramer (2261.45306) is labeled in the inset.

AFM Images of A-RGDV in Rat Plasma. To determine the nanofeatures of A-RGDV in the blood, AFM images in rat plasma were obtained by using the standard method and are shown in Figure 4. As seen, the atomic force microscopy (AFM) images of A-RGDV in water and in rat plasma are nanoparticles of ~50 nm in diameter, while in the image of rat plasma alone no comparable nanoparticle is observed. The observations suggest that even in rat blood the nanoparticles of A-RGDV are still stable and can be optionally delivered in the circulation.

Course of A-RGDV Tetramers Forming Nanoparticles. To identify the conformation of A-RGDV, computer-assisted molecular modeling was performed. The systematic search method produced 30 conformations, and the BEST method produced 195 conformations. The 225 generated conformations were visually examined, and the conformation that matched cross-peak 1

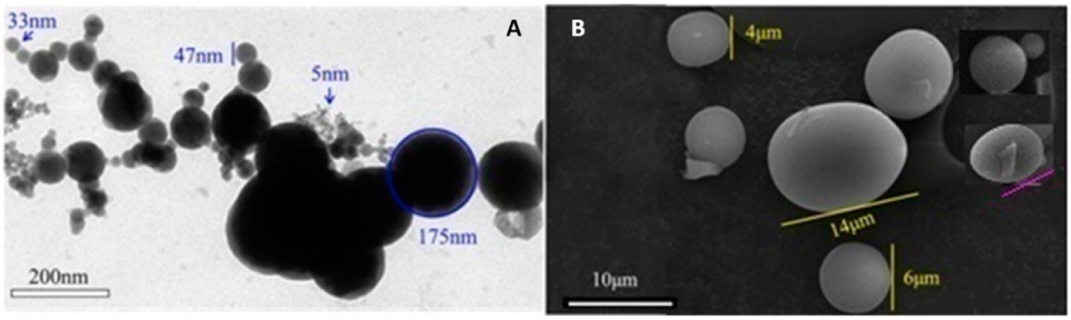

Figure 3. TEM image of A-RGDV in an aqueous solution at pH 7.2 (A) and SEM image in the solid state (B).

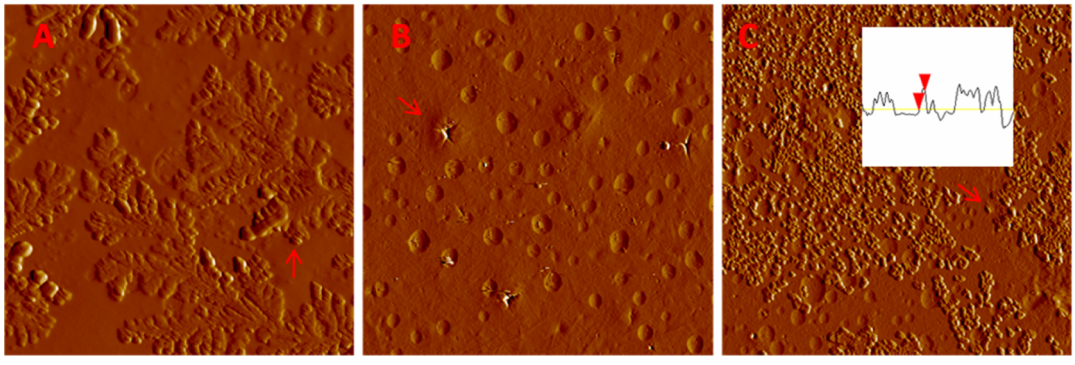

Figure 4. AFM image of A-RGDV in rat plasma. (A) In water A-RGDV exists as nanoparticles of ~50 nm in diameter (denoted with a red arrowhead). (B) In rat plasma alone no comparable nanoparticles are found, only platelets (denoted with a red arrowhead). (C) In rat plasma A-RGDV exists as nanoparticles of ~50 nm in diameter (denoted with a red arrowhead).

of the 2D ROESY NMR spectrum (Figure 1) and had the lowest free energy was selected (Figure 5A). To fulfill the conformation requirements, the intermolecular hydrogen bond interactions defined by cross-peaks 2−4 in the 2D ROESY NMR spectrum, and the ion peak at 2260.63965 in the ESI-MS spectrum (Figure 2), four molecules should be in the vicinity forming a tetramer (Figure 5A). The mesoscale simulation software assisted calculation shows that, employing the tetramer as a building block, 24 tetramers can form a nanoparticle of 5 nm in diameter (Figure 5B). Of the nanoparticles in Figure 3 and Figure 5, the nanoparticle of 5 nm in diameter is the smallest one. Therefore, the smallest nanoparticle contains 24 tetramers.

A-RGDV Releases Aspirin inside a Thrombus. To determine whether RGDV can act as the carrier of aspirin, the change of A-RGDV in plasma and in a thrombus was measured on an ESI-MS spectrometer, and the spectra are given in Figure 6. Figure 6A2 indicates that the ESI-MS spectrum of A-RGDV incubated in rat plasma for 30 min gives the molecular ion peak of A-RGDV (606.23637) only, but no ion peak (444.25338) of RGDV occurs. However, in the ESI-MS spectrum (Figure 6A1) of the rat plasma without A-RGDV (control) no comparable ion peak appears. This indicates that in rat plasma incubated for 30 min A-RGDV does not release aspirin. Figure 6B2 indicates that when A-RGDV is incubated in a rat thrombus for 30 min, the ESI-MS spectrum gives ion peaks of 606.23637 (A-RGDV), 444.25338 (RGDV), 395.13477 (the dimer of aspirin plus Cl^-), and 606.23637 (A-RGDV). This indicates that in the rat thrombus the 30 min incubation drives A-RGDV to release aspirin. On the other hand, the ESI-MS spectrum (Figure 6B1) of the rat thrombus without A-RGDV gives no comparable ion peak.

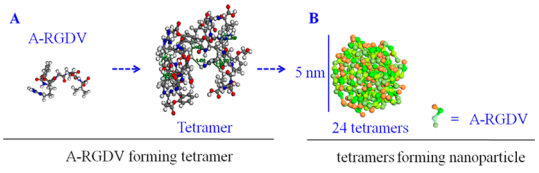

Figure 5. Proposed model of A-RGDV forming tetramers (A) and thereby forming a nanoparticle (B).

Interaction of A-RGDV and GPIIb/IIIa Resulted in the Release of Aspirin. It is well known that the receptor of RGD peptide on the surface of an activated platelet is GPIIb/IIIa. To explore the effect of GPIIb/IIIa on A-RGDV releasing aspirin, aqueous solutions of A-RGDV (100 μg/mL, control), GPIIb/IIIa (0.4 μg/mL, control), and A-RGDV (100 μg/mL) plus GPIIb/IIIa (0.4 μg/mL) were incubated at 37 °C for 30 min, and the ESI-MS spectra were measured (Figure 7). In the ESI-MS spectrum of GPIIb/IIIa (Figure 7A, MS^+) no ion peak related to A-RGDV, RGDV, and aspirin is found. In the ESI-MS spectrum of A-RGDV plus GPIIb/IIIa (Figure 7B, MS^-) ion peaks of 606.23637 (A-RGDV), 564.24836 (A-RGDV losing an acetyl group, intensity = 6×10^7), and 444.22655 (RGDV) are found. The existence of the ion peak of RGDV indicates that the interaction of GPIIb/IIIa with A-RGDV results in A-RGDV releasing aspirin. In the ESI-MS spectrum of A-RGDV (Figure 7C, MS^-) the ion peaks of 606.23637 (A-RGDV) and 564.24782 (A-RGDV losing an acetyl group, intensity = 6×10^8) are found. The intensity of the ion peak of A-RGDV losing an acetyl group in Figure 7B is 10-fold lower than that of the ion peak in Figure 7C, and the decrease of A-RGDV in amount could result from the hydrolyzation of A-RGDV promoted by GPIIb/IIIa.

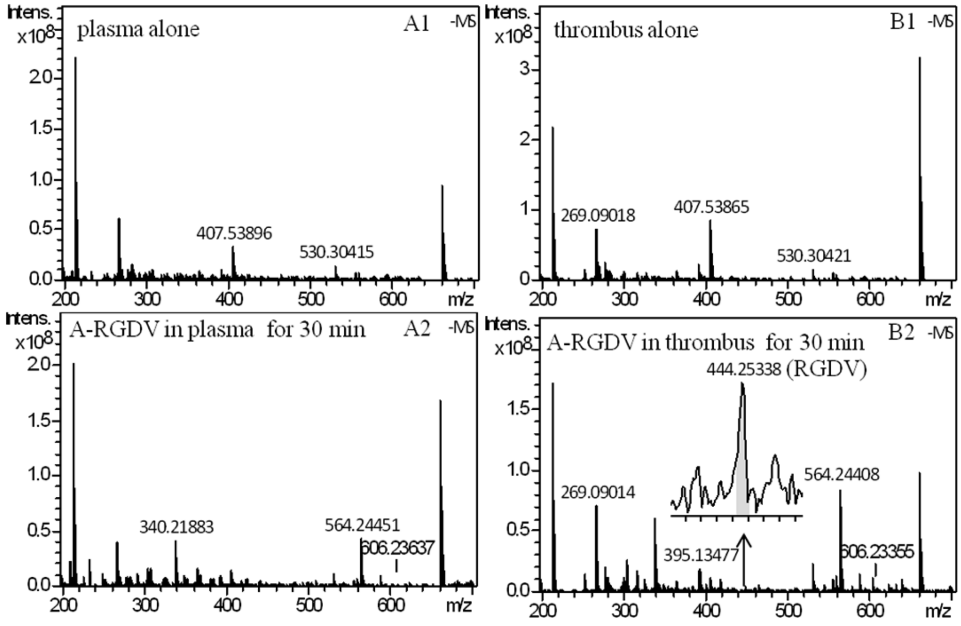

Figure 6. ESI-MS spectra of A-RGDV incubated in rat plasma (A2) or in a thrombus (B2) for 30 min. A1 and B1 are blank plasma and thrombus, respectively.

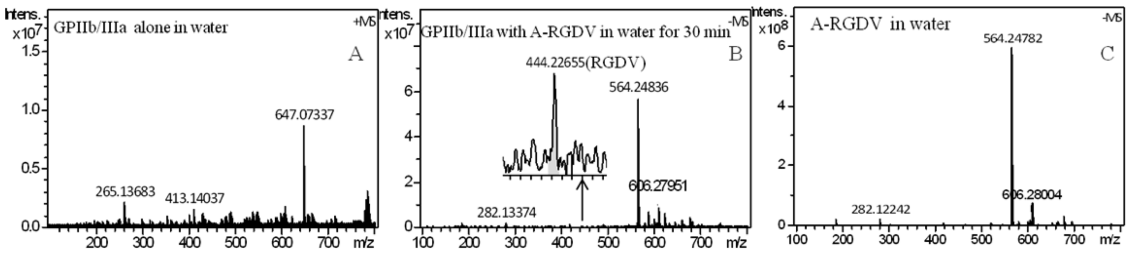

Figure 7. ESI-MS spectra of GPIIb/IIIa in water (A), A-RGDV plus GPIIb/IIIa in water (B), and A-RGDV in water (C). The incubation was performed at 37 °C for 30 min.

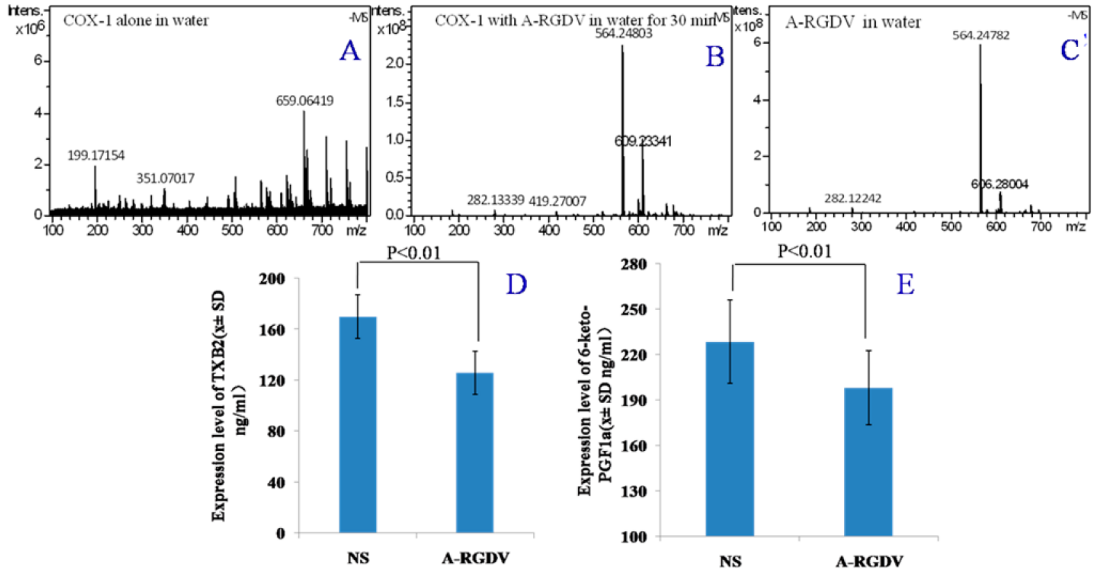

Figure 8. ESI-MS spectra of COX-1 in water (A), COX-1 with A-RGDV in water (B), and A-RGDV in water (C), serum levels of TXB_2 (D), and 6-keto-$PGF_{1\alpha}$ (E). The incubation was performed at 37 °C for 30 min.

Interaction of A-RGDV and COX-1 Resulted in the Conversion of an Acetyl Group. It is well known that cyclooxygenase-1 (COX-1) is one of the key enzymes that promote arachidonic acid (AA), yielding prostaglandin G_2. To explore the effect of COX-1 on the change of A-RGDV, aqueous solutions of COX-1 (2.2 μg/mL, control), A-RGDV (100 μg/mL, control), and A-RGDV (100 μg/mL) plus COX-1 (2.2 μg/mL) were incubated at 37 °C for 30 min, and the ESI-MS spectra were measured (Figure 8). In the ESI-MS spectrum of COX-1 alone (Figure 8A, MS^-) no ion peak related to A-RGDV, RGDV, and aspirin is found. In the ESI-MS spectrum of A-RGDV plus COX-1 (Figure 8B, MS^-) only the ion peak of 564.24803 (A-RGDV losing an acetyl group) is found, while in the ESI-MS spectrum of A-RGDV alone (Figure 8C, MS^-) the ion peaks of 606.23637 (A-RGDV) and 564.24803 (A-RGDV losing an acetyl group) are found. This suggests that the interaction of A-RGDV and COX-1 results in the disappearance of A-RGDV, and it may be attributed to A-RGDV blocking COX-1. To evidence the blockage of COX-1, the serum levels of rat thromboxane B_2 (TXB_2) and 6-keto-$PGF_{1\alpha}$ were measured according to the manufacture's guidance using the rat thromboxane B_2 (TXB_2) ELISA kit (HuaYi Biotechnology Co., Ltd.) and the rat 6-keto-$PGF_{1\alpha}$ ELISA kit (HuaYi Biotechnology Co., Ltd.), respectively, and the data are also shown in Figure 8 (D and E). A-RGDV significantly decreases the serum levels of both TXB_2 and 6-keto-$PGF_{1\alpha}$, supporting the blockage of COX-1-mediated AA metabolism. The methods to determine TXB_2 and 6-keto-$PGF_{1\alpha}$ are provided in the Supporting Information.

A-RGDV Selectively Inhibiting AA-Induced Antiplatelet Aggregation. In the antiplatelet aggregation model the *in vitro* activities of A-RGDV inhibiting adenosine diphosphate (ADP)-, arachidonic acid (AA)-, and thrombin (TH)-induced platelet aggregation were determined, and the data are shown in Figure 9A. Even though 10^{-4} M aspirin and RGDV did not inhibit TH- and AA-induced platelet aggregation, the inhibitory capability of A-RGDV against TH- and AA-induced platelet aggregation is 14.65% and 44.8%, respectively. This means that in terms of TH- and AA-induced platelet aggregation the activity of A-RGDV is higher than that of aspirin and RGDV. The inhibition of 10^{-4} M aspirin, RGDV, and A-RGDV against ADP-induced platelet aggregation is 24.3%, 44.6%, and 33.1%, respectively. This means that for ADP-induced platelet aggregation the activity of A-RGDV is less than that of RGDV. Of the three

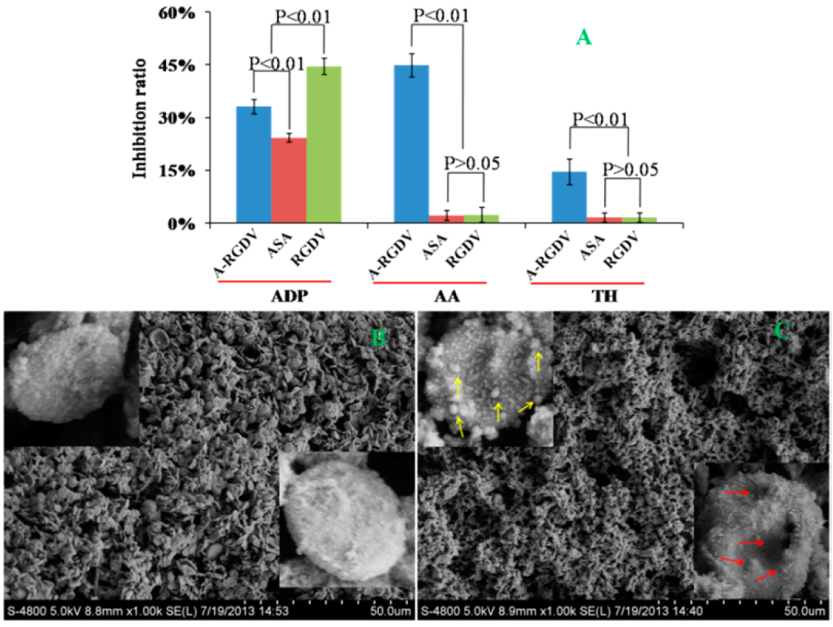

Figure 9. Inhibition ratio of 10^{-4} M A-RGDV, ASA (aspirin), and RGDV against ADP-, AA-, and TH-induced platelet aggregation (A), ESM image of resting rat platelets (B), and ESM image of AA-activated rat platelets with A-RGDV (10^{-4} M, C). The data are represented as mean ± SD%, n = 6. In the magnified image the yellow arrowheads point to the nanoparticles adhered on the surface of the activated platelet, and the red arrowheads point to nanoparticles in the course of endocytosis.

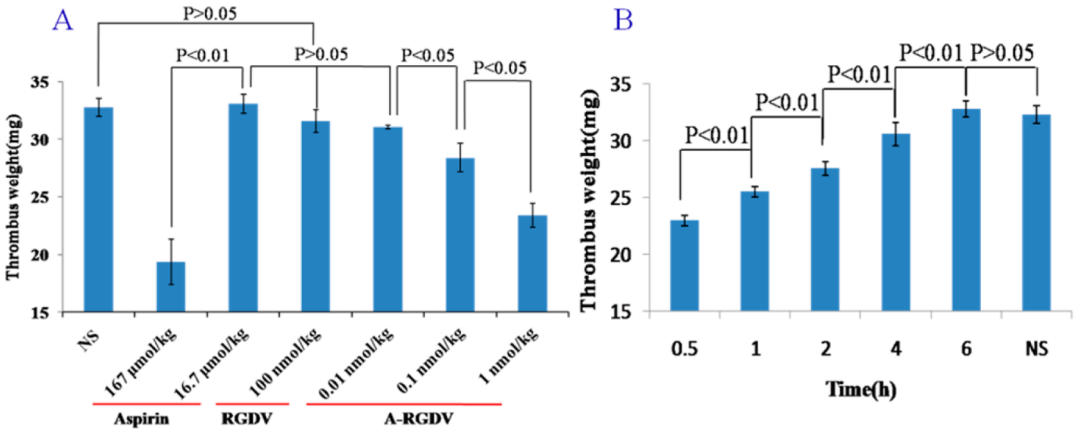

Figure 10. Dose-dependent antithrombotic activity (A, n = 12) and time-dependent antithrombotic activity (B, n = 5) of A-RGDV. Thrombus weight of the treated rat is represented as the mean ± SD mg, NS = normal saline.

aggregators, A-RGDV selectively inhibits AA-induced platelet aggregation, and its activity is ~23-fold higher than that of aspirin and RGDV.

To further explore the effect of the nanoparticles on AA-induced platelet aggregation, the ESM images of resting rat platelets and AA-activated rat platelets with 10^{-4} M A-RGDV were obtained and are shown in Figure 9B and C. As seen in Figure 9B, in the resting condition the surface image of a magnified rat platelet is relatively smooth. In contrast, the surface images of AA-activated rat platelet with pretreatment of A-RGDV show a great deal of nanoparticles. One magnified image labeled with yellow arrowheads shows that numerous nanoparticles adhere on the surface. Another magnified image labeled with red arrowheads shows that some of the nanoparticles are in the course of endocytosis, and some of the nanoparticles are inside the platelet membrane breach. These interactions of A-RGDV and the activated platelets mirrored by ESM images should support A-RGDV inhibiting AA-induced platelet aggregation.

***In Vivo* Antithrombotic Activity of A-RGDV.** The *in vivo* antithrombotic activities of aspirin (reference control, 16.7 and 167 μmol/kg doses), RGDV (reference control, 100 nmol/kg of dose), and A-RGDV (1, 0.1, and 0.01 nmol/kg doses) were evaluated on a rat model, represented with thrombus weight, and the data are shown in Figure 10A. At a 16.7 μmol/kg dose, aspirin exhibits no antithrombotic action. At a 100 nmol/kg dose, RGDV also does not inhibit the rats from forming

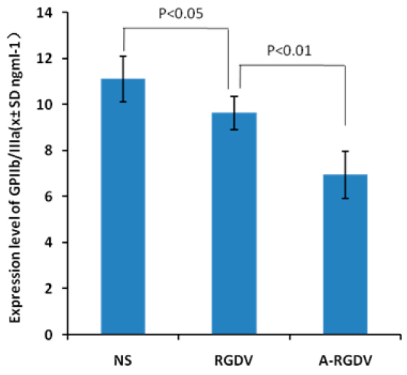

Figure 11. Effects of RGDV and A-RGDV on the expression of GPIIb/IIIa. The concentration of RGDV and A-RGDV is 0.4 mM. Data are represented as mean ± SD ng mL^{-1}, NS = normal saline, n = 4.

thrombi. However, at doses of 0.1 and 1 nmol/kg, A-RGDV effectively inhibits thrombosis in the treated rats, and the antithrombotic activity increases in a dose-dependent manner. The comparison of the nonresponsive dose of aspirin (16.7 μmol/kg) and one of the effective doses of A-RGDV (0.1 nmol/kg) indicates that the efficacy of A-RGDV is 16 700-fold higher than that of aspirin. The extraordinarily high inhibition could result from A-RGDV targeting the activated platelets, releasing aspirin to activated platelets, and consequently blocking thrombus formation.

In order to explore how long A-RGDV is capable of maintaining a sustained effect, the *in vivo* time-dependent antithrombotic activities of 1 nmol/kg of A-RGDV were assayed on the same model, the thrombus weights of the rats 0.5, 1, 2, 4, and 6 h after administration were weighed, and the results are shown in Figure 10B. The data indicate that at a 1 nmol/kg oral dose A-RGDV effectively inhibits thrombus formation in treated rats. With the dosing time prolonged from 0.5 to 6 h the activity steadily decreases, and 6 h after administration A-RGDV no longer possesses antithrombotic action. These characterize the time dependence of the *in vivo* action of A-RGDV and give a 1 nmol/kg dose of oral A-RGDV a 4 h effective time *in vivo*. In the same conditions the effective time of 167 μmol/kg of aspirin was only 0.5 h.

Effect of A-RGDV on GPIIb/IIIa Expression. To clarify the effect of RGDV on the interaction of A-RGDV with the receptor GPIIb/IIIa, the expression levels of GPIIb/IIIa of RGDV- and A-RGDV-treated platelets were examined with ELISA experiments, and the data are shown in Figure 11. As seen, at a 0.4 mM concentration both RGDV and A-RGDV significantly inhibit the expression of GPIIb/IIIa. On the other hand, the inhibition activity of A-RGDV is significantly higher than that of RGDV. The comparisons mean that GPIIb/IIIa is the receptor of both RGDV and A-RGDV, and the conjugation of aspirin and RGDV significantly enhances the interaction of RGDV with GPIIb/IIIa.

CONCLUSIONS

In contrast to the nanoparticles that consisted of macromolecules such as biomaterials, engineered materials, and pharmaceutical materials,[48−51] the present nanoparticles consisted of a small-molecule, aspirin-linked tetrapeptide. In normal blood vessels the nanoparticles were optionally delivered in the blood without interfering with the integrated nanostructure and molecular structure. If the vascular endothelium is injured and the platelets are activated, the nanoparticles will target the injured site, interact with the activated platelets, bind the receptor GPIIb/IIIa, release aspirin, and block the conversion of AA into PGG_2. Thereby, A-RGDV functions as a delivery system of aspirin, and RGDV functions as the target carrier of aspirin and miraculously increases the efficacy of aspirin in inhibiting thrombosis. Thus, the present paper provided a strategy of RGD peptide carrying aspirin to the thrombus, releasing aspirin inside the thrombus, and finally avoiding aspirin resistance and nonresponse.

MATERIALS AND METHODS

^{1}H NMR spectra were recorded on a Bruker 800 MHz spectrometer with DMSO-d_6 or $CDCl_3$ as the solvent and tetramethylsilane as an internal standard. ESI-MS was tested on a ZQ 2000 (Waters, US) and a SolariX FT-ICR mass spectrometer (Bruker Daltonik) consisting of an ESI/MALDI dual ion source and 9.4 T superconductive magnet.

Male Wister rats were purchased from Animal Center of Peking University. The described assessments were performed based on a protocol reviewed and approved by the ethics committee of Capital Medical University. The committee assures that the welfare of the rats was maintained in accordance with the requirements of the animal welfare act and in accordance with the guide for care and use of laboratory animals. The statistical analysis of all the biological data was carried out by use of an ANOVA test with $p < 0.05$ as significant cutoff.

Protective amino acids with L-configuration were purchased from Sigma Chemical Co. COX-1 and GPIIb/IIIa (analytically pure) were purchased from Sigma-Aldrich Co. (LLC) and Cusabio Biotech Co. (Ltd), respectively. Sodium citrate (analytically pure) was purchased from Beijing Chemical Factory, and acetonitrile (spectroscopically pure) was purchased from Thermo Fisher Scientific Inc.

Synthesis. As indicated in Scheme 1 of the Supporting Information, A-RGDV was prepared from aspirin and the corresponding protective amino acids. In brief, the partial protective RGDV, *i.e.*, Arg(NO_2)-Gly-Asp-(OBzl)-Val-OBzl (**1**), was prepared by a solution method and a "2 + 2" strategy. Under the general conditions aspirin was coupled with **1** to give *N*-(2-acetyloxybenzoyl)-Arg((=NO_2)-Gly-Asp(OBzl)-Val-OBzl (**2**). The hydrogenation of **2** provided *N*-(2-acetyloxybenzoyl)-Arg-Gly-Asp-Val (A-RGDV). The total yield was 12%. The procedure and the yield of each reaction, as well as the physical and chemical data of all intermediates and products, are provided as Supporting Information.

3D Structure Generation and Aggregation Model. The 2D structure of A-RGDV was sketched with ChemDraw Ultra 10.0. The 3D structure was created and energy minimized until the minimum rms reached 0.001 in Chem3D Ultra 10.0. Then the 3D structure was energy minimized with Discovery Studio 2.1 with the MMFF force field. The energy-minimized conformation was utilized as

the starting conformation for conformation generation of A-RGDV. The energy-minimized conformations were sampled in the whole conformational space *via* a systematic search method and the BEST method in Discovery Studio 2.1. Both the systematic search and BEST methods were performed with the SMART minimizer using the CHARMM force field. The energy threshold was set to 20 kcal/mol at 300 K. The maximum minimization steps was set to 200, and the minimization of the rms gradient was set to 0.1 Å. The maximum generated conformations were set to 255 with an rmsd cutoff of 0.2 Å. According to the 3D structure and the intermolecular interactions identified with the ROESY 2D NMR spectrum and the ESI-MS spectrum of A-RGDV, the present aggregation model was proposed.

Maldi-Mass Test. The ESI mass spectrum was acquired using a SolariX FT-ICR mass spectrometer (Bruker Daltonics) consisting of an ESI/MALDI dual ion source and 9.4 T superconductive magnet. The measurement was carried out in the positive Maldi ion mode. A smartbeam-II laser (wavelength, 355 nm; focus setting, medium; repetition rate, 1000 Hz) was used as the ion source. qCID mass was set to 2260.63956 *m/z*, and the isolation window was 5 *m/z*. Data were acquired using SolariXcontrol software. Spectral data were processed with DataAnalysis software (Bruker Daltonics).

TEM Test. The shape and size examinations of the nanospecies of A-RGDV were performed on a transmission electron microscope (JSM-6360 LV, JEOL, Tokyo, Japan). An aqueous solution of pH 7.2 of A-RGDV was dripped onto a Formvar-coated copper grid, and then a drop of anhydrous ethanol was added to promote water removal. The grid was first allowed to thoroughly dry in air and was then heated at 35 °C for 24 h. The samples were viewed under the TEM. The shape and size distribution of the nanospecies were determined from counting over 100 species in randomly selected regions on the TEM copper grid. All the determinations were carried out in triplicate grids. The TEM was operated at 80 kV, electron beam accelerating voltage. Images were recorded on an imaging plate (Gatan Bioscan Camera model 1792) with 20 eV energy windows at 6000−400 000× and were digitally enlarged.

SEM Test. The shape and size of the nanospecies of the lyophilizing powders of a solution of A-RGDV in ultrapure water (1.2 mM) were measured on a scanning electron microscope (SEM, JEM-1230, JEOL, Tokyo, Japan) at 50 kV. The lyophilizing powders were attached to a copper plate *via* double-sided tape (Euromedex, France). The specimens were coated with 20 nm of gold−palladium using a JEOL JFC-1600 Auto Fine Coater. The coater was operated at 15 kV, 30 mA, and 200 mTorr (argon) for 60 s. The shape and size distribution of the nanoparticles were measured by counting over 100 particles in randomly selected regions on the SEM alloy. All the measurements were performed in triplicate grids. The images were recorded on an imaging plate (Gatan Bioscan Camera model 1792) with 20 eV energy windows at 100−10 000× and were digitally enlarged.

AFM Test. Atomic force microscopy images were obtained by using the contact mode on a Nanoscope 3D AFM (Veeco Metrology, Santa Barbara, CA, USA) under ambient conditions. Samples of A-RGDV in water or in rat plasma (8.0×10^{-7} M at pH 7.2) were used for recording the images.

***In Vitro* Antiplatelet Aggregation Assay.** An H-10 cell counter was used to determine the platelet count, and a two-channel Chronolog Aggregometer was used to evaluate platelet aggregation. After collection, the pig blood was centrifuged at 100*g* for 10 min, and the platelet-rich plasma (PRP) was removed. The remaining blood was centrifuged for an additional 10 min at 1500*g* to prepare platelet-poor plasma (PPP). The final platelet count of the citrated plasma samples was adjusted to 2×10^8 platelets/mL with autologous PPP. To an optical aggregometry testing tube were added 0.5 mL of the adjusted plasma sample and 5 μL of NS or 5 μL of the solution of A-RGDV, RGDV, or aspirin in NS. After adjustment of the baseline, 5 μL of the solution of adenosine diphosphate in NS (final concentration 10 μM), 5 μL of the solution of arachidonic acid in NS (final concentration 350 μM), or 50 μL of the solution of thrombin in NS (final concentration 0.1 U/mL) was added, and aggregation was measured at 37 °C for 5 min. The effects of A-RGDV, RGDV, or aspirin (final concentration 10^{-4} M) on ADP-, AA-, or TH-induced platelet aggregation were observed. The maximal rate of platelet aggregation (A_m%) was represented by the peak height of the aggregation curve. The inhibition rate was calculated by % inhibition = [(A_m% of NS, 50.00 ± 3.21%) − (A_m% of A-RGDV)]/(A_m% of NS, 50.00 ± 3.21%).

***In Vivo* Antithrombotic Assay.** Aspirin (positive control) and A-RGDV were dissolved in NS (vehicle) before the administration and kept in an ice bath for use. Male Wistar rats (12 for each group) weighing 255−302 g were anesthetized with pentobarbital sodium (80.0 mg/kg, ip), and the right carotid artery and left jugular vein were separated. A weighed 6 cm thread was inserted into the middle of a polyethylene tube. The polyethylene tube was filled with a solution of heparin sodium in NS (50 IU/mL), and one end was inserted into the left jugular vein. From the other end of the polyethylene tube the solution of heparin sodium in NS was injected as the anticoagulant; then NS alone, a solution of A-RGDV in NS, or a solution of aspirin in NS was injected, and this end was inserted into the right carotid artery. The blood was allowed to flow from the right carotid artery to the left jugular vein through the polyethylene tube for 15 min. The thread was removed to obtain the weight of the wet thrombus. The statistical analysis of the data was carried out by use of an ANOVA statistical test. The significant differences were determined using a *p*-value of less than 0.05 ($p < 0.05$).

GPIIb/IIIa Levels of A-RGDV-Treated Platelets. GPIIb/IIIa levels of the platelets were measured on citrated rat blood samples by an enzyme immunoassay according to the manufacturer's instructions (rat platelet membrane glycoprotein ELISA kit, RAPIDBIO Co., USA). Rat blood was collected in an aqueous solution of 3.8% sodium citrate (1:9, v/v) and immediately centrifuged at 160*g* for 15 min to collect platelet-rich plasma. To 600 μL of PRP was added 5400 μL of the diluent (from the kit) to prepare the PRP sample. A-RGDV or RGDV was dissolved in NS to prepare the A-RGDV or RGDV solution (0.4 mM). To 960 μL of the PRP sample was added 20 μL of A-RGDV or RGDV solution (0.4 mM), and the reaction mixture incubated at 37 °C for 5 min, to which 20 μL of AA in NS (0.15 mg/mL) was added. The reaction mixture was then incubated at 37 °C for 3 min. This is the test sample, *i.e.*, the A-RGDV- or RGDV-treated PRP sample. To 960 μL of the PRP sample was added 20 μL of NS, and the mixture was incubated at 37 °C for 5 min, to which 20 μL of AA in NS (0.15 mg/mL) was added. The reaction mixture was then incubated at 37 °C for another 3 min. This is the blank control sample, *i.e.*, the NS-treated PRP sample. To the control well and the test well in the 96-well plate coated with the enzyme were added 50 μL of the NS-treated PRP sample and 50 μL of the A-RGDV- or RGDV-treated PRP sample, respectively. At 37 °C the plate was incubated for 30 min. Upon the removal of the solvent, the wells were washed with washing solution (from the kit, 300 μL × 5). To the control well was added 50 μL of NS, to the test well was added 50 μL of enzyme labeling solution (from the kit), and the plate was incubated at 37 °C for 30 min. Upon the removal of the solvent, the wells were washed with washing solution (from the kit, 300 μL × 5). To each well were successively added 50 μL of chromogen solution A and 50 μL of chromogen solution B (from the kit), the solution was gently mixed and colored at 37 °C and protected from light for 15 min. To each well was added 50 μL of the stop solution (from the kit) to stop the coloration for 10 min. At 450 nm the OD value of each well was tested and the GPIIb/IIIb level was calculated according to the standard samples (from the kit). The samples could also be kept at −20 °C for no more than 10 days before analysis.[25,26]

Metabolism in Blood and Thrombus. The orbit blood of rat was sampled with or without an aqueous solution of sodium citrate (3.8%). To 200 μL of the blood samples or 200 μL of distilled water was added 50 μL of an aqueous solution of A-RGDV (3 μM). After the coagulation of the blood without an aqueous solution of sodium citrate the samples were incubated at 37 °C for 15 or 30 min. The blood and the water samples were centrifuged for 10 min (10 000 rpm), and then 10 μL of the supernatant was taken for the ESI-MS experiment. The thrombus from the blood without the aqueous solution of sodium citrate was ground and centrifuged for 10 min (10 000 rpm), and then 10 μL of the supernatant was taken for the ESI-MS experiment.

Interaction of A-RGDV and GPIIb/IIIa. The aqueous solution of GPIIb/IIIa alone (200 μL, 0.4 μg/mL), A-RGDV alone (200 μL, 100 μg/mL), or the thoroughly mixed aqueous solution of A-RGDV (200 μL,100 μg/mL) and GPIIb/IIIa (200 μL, 0.4 μg/mL) was incubated at 37 °C for 30 min. Then 10 μL of the solution was used for the ESI-MS measurement (dry gas, 4 L/min; nebulizer gas, 0.5 bar; capillary, 4000 V; end plate offset, −500 V).

Interaction of A-RGDV and COX-1. The aqueous solution of COX-1 alone (200 μL, 2.2 μg/mL), A-RGDV alone (200 μL, 100 μg/mL), or the thoroughly mixed aqueous solution of A-RGDV (200 μL, 100 μg/mL) and COX-1 (200 μL, 2.2 μg/mL) was incubated at 37 °C for 30 min. Then 10 μL of the solution was used for the ESI-MS measurement (dry gas, 4 L/min; nebulizer gas, 0.5 bar; capillary, 4000 V; end plate offset, −500 V).

Conflict of Interest: The authors declare no competing financial interest.

Acknowledgment. This work was supported by the Engineering Research Center of Endogenous Prophylactic of Ministry of Education of China, by PHR (IHLB), by the National Natural Science Foundation (81172930, 81273379, and 81202412), by Beijing Natural Science Foundation (7122023), and by Special Project (2011ZX09302-007-01) of China. We thank Neotrident Technology Ltd. for providing mesoscale simulation software (Materials Studio 6.1).

Supporting Information Available: Additional figures as described in the text; additional experimental details. This material is available free of charge *via* the Internet at http://pubs.acs.org.

REFERENCES AND NOTES

1. Castro, P.; Nasser, H.; Abrahão, A.; Dos Reis, L. C.; Riça, I.; Valença, S. S.; Rezende, D. C.; Quintas, L. E.; Cavalcante, M. C.; Porto, L. C.; *et al.* Aspirin and Indomethacin Reduce Lung Inflammation of Mice Exposed to Cigarette Smoke. *Biochem. Pharmacol.* **2009**, *77*, 1029–1039.
2. Liu, J. Y.; Yang, J.; Inceoglu, B.; Qiu, H.; Ulu, A.; Hwang, S. H.; Chiamvimonvat, N.; Hammock, B. D. Inhibition of Soluble Epoxide Hydrolase Enhances the Anti-Inflammatory Effects of Aspirin and 5-Lipoxygenase Activation Protein Inhibitor in a Murine Model. *Biochem. Pharmacol.* **2010**, *79*, 880–887.
3. Cholette, J. M.; Mamikonian, L.; Alfieris, G. M.; Blumberg, N.; Lerner, N. B.; Jill, M.; Cholette, L. M.; George, M.; Alfieris, N. B.; Norma, B. L. Aspirin Resistance Following Pediatric Cardiac Surgery. *Thromb. Res.* **2010**, *126*, 200–206.
4. Wong, S.; Appleberg, M.; Ward, C. M.; Lewis, D. R. Aspirin Resistance in Cardiovascular Disease: A Review. *Eur. J. Vasc. Endovasc. Surg.* **2004**, *27*, 456–465.
5. Carmignani, L.; Picozzi, S.; Bozzini, G.; Negri, E.; Ricci, C.; Gaeta, M.; Pavesi, M. Transrectal Ultrasound-Guided Prostate Biopsies in Patients Taking Aspirin for Cardiovascular Disease: A Meta-Analysis. *Transfus. Apheresis Sci.* **2011**, *45*, 275–280.
6. Berger, J. S.; Lala, A.; Krantz, M. J.; Baker, G. S.; Hiatt, W. R. Aspirin for the Prevention of Cardiovascular Events in Patients without Clinical Cardiovascular Disease: A Meta-Analysis of Randomized Trials. *Am. Heart. J.* **2011**, *162*, 115–124.e2.
7. Lamotte, M.; Piñol, C.; Brotons, C.; Annemans, L.; Guardiola, E.; Evers, T.; Kubin, M. Health Economic Evaluation of Low-Dose Acetylsalicylic Acid in the Primary Prevention of Cardiovascular Disease. *Rev. Esp. Cardiol.* **2006**, *59*, 807–815.
8. Chaturvedi, S. Acetylsalicylic Acid + Extended-Release Dipyridamole Combination Therapy for Secondary Stroke Prevention. *Clin. Ther.* **2008**, *30*, 1196–1205.
9. Meyer, D. M.; Albright, K. C.; Allison, T. A.; Grotta, J. C. LOAD: A Pilot Study of the Safety of Loading of Aspirin and Clopidogrel in Acute Ischemic Stroke and Transient Ischemic Attack. *J. Stroke Cerebrovasc. Dis.* **2008**, *17*, 26–29.
10. Rey, E.; Rivard, G. E. Is Testing for Aspirin Response Worthwhile in High-Risk Pregnancy? *Eur. J. Obstet. Gynecol. Reprod. Biol.* **2011**, *157*, 38–42.
11. Perneby, C.; Vahter, M.; Akesson, A.; Bremme, K.; Hjemdahl, P. Thromboxane Metabolite Excretion during Pregnancy - Influence of Preeclampsia and Aspirin Treatment. *Thromb. Res.* **2011**, *127*, 605–606.
12. Schrör, K. Pharmacology and Cellular/Molecular Mechanisms of Action of Aspirin and Non-Aspirin NSAIDs in Colorectal Cancer. *Best Pract. Res. Clin. Gastroenterol.* **2011**, *25*, 473–484.
13. Lim, W. Y.; Chuah, K. L.; Eng, P.; Leong, S. S.; Lim, E.; Lim, T. K.; Ng, A.; Poh, W. T.; Tee, A.; Teh, M.; *et al.* Aspirin and Non-Aspirin Non-Steroidal Anti-Inflammatory Drug Use and Risk of Lung Cancer. *Lung Cancer* **2012**, *77*, 246–251.
14. Garcia-Albeniz, X.; Chan, A. T. Aspirin for the Prevention of Colorectal Cancer. *Best Pract. Res. Clin. Gastroenterol.* **2011**, *25*, 461–472.
15. Yassine, H. N.; Davis-Gorman, G.; Stump, C. S.; Thomson, S. S.; Peterson, J.; McDonagh, P. F. Clinical Determinants of Aspirin Resistance in Diabetes. *Diabetes Res. Clin. Pract.* **2010**, *90*, e19–e21.
16. Zhang, C.; Sun, A.; Zhang, P.; Wu, C.; Zhang, S.; Fu, M.; Wang, K.; Zou, Y.; Ge, J. Aspirin for Primary Prevention of Cardiovascular Events in Patients with Diabetes: A Meta-Analysis. *Diabetes Res. Clin. Pract.* **2010**, *87*, 211–218.
17. Lin, L.; Cao, J.; Fan, L.; Hu, G.; Hu, Y.; Zhu, B.; Li, X.; Wang, H.; Bai, J.; Shi, H. Prevalence and Risk Factors for Aspirin Resistance in Elderly Patients with Type 2 Diabetes. *Int. J. Gerontol.* **2011**, *5*, 112–116.
18. Duzenli, M. A.; Ozdemir, K.; Aygul, N.; Soylu, A.; Tokac, M. Comparison of Increased Aspirin Dose *versus* Combined Aspirin plus Clopidogrel Therapy in Patients with Diabetes Mellitus and Coronary Heart Disease and Impaired Antiplatelet Response to Low-Dose Aspirin. *Am. J. Cardiol.* **2008**, *102*, 396–400.
19. Pomponi, M. F.; Gambassi, G.; Pomponi, M.; Di Gioia, A.; Masullo, C. Why Docosahexaenoic Acid and Aspirin Supplementation Could Be Useful in Women as a Primary Prevention Therapy against Alzheimer's Disease? *Ageing Res. Rev.* **2011**, *10*, 124–131.
20. Caraci, F.; Copani, A.; Nicoletti, F.; Drago, F. Depression and Alzheimer's Disease: Neurobiological Links and Common Pharmacological Targets. *Eur. J. Pharmacol.* **2010**, *626*, 64–71.
21. Le Guyader, A.; Pacheco, G.; Seaver, N.; Davis-Gorman, G.; Copeland, J.; McDonagh, P. F. Inhibition of Platelet GPIIb-IIIa and P-Selectin Expression by Aspirin Is Impaired by Stress Hyperglycemia. *J. Diabetes Complications* **2009**, *23*, 65–70.
22. Shaker, M.; Lobb, A.; Jenkins, P.; O'Rourke, D.; Takemoto, S. K.; Sheth, S.; Burroughs, T.; Dykewicz, M. S. An Economic Analysis of Aspirin Desensitization in Aspirin-Exacerbated Respiratory Disease. *J. Allergy Clin. Immunol.* **2008**, *121*, 81–87.
23. Stevenson, D. D.; Simon, R. A. Selection of Patients for Aspirin Desensitization Treatment. *J. Allergy Clin. Immunol.* **2006**, *118*, 801–804.
24. Wong, S.; Appleberg, M.; Ward, C. M.; Lewis, D. R. Aspirin Resistance in Cardiovascular Disease: A Review. *Eur. J. Vasc. Endovasc. Surg.* **2004**, *27*, 456–465.
25. Poulsen, T. S.; Kristensen, S. R.; Korsholm, L.; Haghfelt, T.; Jørgensen, B.; Licht, P. B.; Mickley, H. Variation and Importance of Aspirin Resistance in Patients with Known Cardiovascular Disease. *Thromb. Res.* **2007**, *120*, 477–484.
26. Seok, J. I.; Joo, I. S.; Yoon, J. H.; Choi, Y. J.; Lee, P. H.; Huk, K.; Bang, O. Y. Can Aspirin Resistance be Clinically Predicted in Stroke Patients? *Clin. Neurol. Neurosurg.* **2008**, *110*, 110–116.
27. Hobikoglu, G. F.; Norgaz, T.; Aksu, H.; Ozer, O.; Erturk, M.; Destegul, E.; Akyuz, U.; Unal Dai, S.; Narin, A. The Effect of Acetylsalicylic Acid Resistance on Prognosis of Patients Who have Developed Acute Coronary Syndrome during Acetylsalicylic Acid Therapy. *Can. J. Cardiol.* **2007**, *23*, 201–206.
28. Pui-Yin, L.; Wai-Hong, C.; William, N.; Xi, C.; Jeanette, Y. K.; Hung-Fat, T.; Chu-Pak, L. Low-Dose Aspirin Increases Aspirin Resistance in Patients with Coronary Artery Disease. *Am. J. Med.* **2005**, *118*, 723–727.

29. Cholette, J. M.; Mamikonian, L.; Alfieris, G. M.; Blumberg, N.; Lerner, N. B. Aspirin Resistance Following Pediatric Cardiac Surgery. *Thromb. Res.* **2010**, *126*, 200–206.
30. Watala, W.; Golanski, J.; Pluta, J.; Boncler, M.; Rozalski, M.; Luzak, B.; Kropiwnicka, A.; Drzewoski, J. Reduced Sensitivity of Platelets from Type 2 Diabetic Patients to Acetylsalicylic Acid (Aspirin)-Its Relation to Metabolic Control. *Thromb. Res.* **2004**, *113*, 101–113.
31. Boncler, M.; Gresner, P.; Nocun, M.; Rywaniak, J.; Dolnik, M.; Rysz, J.; Wilk, R.; Czyz, M.; Markuszewski, L.; Banach, M.; *et al.* Elevated Cholesterol Reduces Acetylsalicylic Acid-Mediated Platelet Acetylation. *Biochim. Biophys. Acta* **2007**, *1770*, 1651–1659.
32. Chapman, M. J. From Pathophysiology to Targeted Therapy for Atherothrombosis: A Role for the Combination of Statin and Aspirin in Secondary Prevention. *Pharmacol. Ther.* **2007**, *113*, 184–196.
33. Juzwa, M.; Rusin, A.; Zawidlak-Wegrzyńska, B.; Krawczyk, Z.; Obara, I.; Jedliński, Z. Oligo(3-Hydroxybutanoate) Conjugates with Acetylsalicylic Acid and their Antitumour Activity. *Eur. J. Med. Chem.* **2008**, *43*, 1785–1790.
34. Jenneck, C.; Juergens, U.; Buecheler, M.; Novak, N. Pathogenesis, Diagnosis, and Treatment of Aspirin Intolerance. *Ann. Allergy, Asthma, Immunol.* **2007**, *99*, 13–21.
35. White, A.; Ludington, E.; Mehra, P.; Stevenson, D. D.; Simon, R. A. Effect of Leukotriene Modifier Drugs on the Safety of Oral Aspirin Challenges. *Ann. Allergy, Asthma, Immunol.* **2006**, *97*, 688–693.
36. Zhang, Z.; Lai, Y.; Yu, L.; Ding, J. Effects of Immobilizing Sites of RGD Peptides in Amphiphilic Block Copolymers on Efficacy of Cell Adhesion. *Biomaterials* **2010**, *31*, 7873–7882.
37. Hennessy, K. M.; Clem, W. C.; Phipps, M. C.; Sawyer, A. A.; Shaikh, F. M.; Bellis, S. L. The Effect of RGD Peptides on Osseointegration of Hydroxyapatite Biomaterials. *Biomaterials* **2008**, *29*, 3075–3083.
38. Rafiuddin Ahmed, M.; Jayakumar, R. Peripheral Nerve Regeneration in RGD Peptide Incorporated Collagen Tubes. *Brain Res.* **2003**, *993*, 208–216.
39. Kalinina, S.; Gliemann, H.; López-García, M.; Petershans, A.; Auernheimer, J.; Schimmel, T.; Bruns, M.; Schambony, A.; Kessler, H.; Wedlich, D.; Isothiocyanate-Functionalized, R. G. D. Peptides for Tailoring Cell-Adhesive Surface Patterns. *Biomaterials* **2008**, *29*, 3004–3013.
40. Hwang, D. S.; Sim, S. B.; Cha, H. J. Cell Adhesion Biomaterial Based on Mussel Adhesive Protein Fused with RGD Peptide. *Biomaterials* **2007**, *28*, 4039–4046.
41. Hagisawa, K.; Nishioka, T.; Suzuki, R.; Takizawa, T.; Maruyama, K.; Takase, B.; Ishihara, M.; Kurita, A.; Yoshimoto, N.; Ohsuzu, F.; *et al.* Enhancement of Ultrasonic Thrombus Imaging Using Novel Liposomal Bubbles Targeting Activated Platelet Glycoprotein IIb/IIIa Complex - *In Vitro* and *In Vivo* Study. *Int. J. Cardiol.* **2011**, *152*, 202–206.
42. Sánchez-Cortés, J.; Mrksich, M. The Platelet Integrin αIIbβ3 Binds to the RGD and AGD Motifs in Fibrinogen. *Chem. Biol.* **2009**, *16*, 990–1000.
43. Barre, D. E. Arginyl-Glycyl-Aspartyl (RGD) Epitope of Human Apolipoprotein (a) Inhibits Platelet Aggregation by Antagonizing the IIb Subunit of the Fibrinogen (GPIIb/IIIa) Receptor. *Thromb. Res.* **2007**, *119*, 601–607.
44. Kupczyk, M.; Kurmanowska, Z.; Kupryś-Lipińska, I.; Bocheńska-Marciniak, M.; Kuna, P. Mediators of Inflammation in Nasal Lavage from Aspirin Intolerant Patients after Aspirin Challenge. *Resp. Med.* **2010**, *104*, 1404–1409.
45. Vaidya, B.; Nayak, M. K.; Dash, D.; Agrawal, G. P.; Vyas, S. P. Development and Characterization of Site Specific Target Sensitive Liposomes for the Delivery of Thrombolytic Agents. *Int. J. Pharmaceut.* **2011**, *403*, 254–261.
46. Lukasik, M.; Dworacki, G.; Michalak, S.; Kufel-Grabowska, J.; Golanski, J.; Watala, C.; Kozubski, W. Aspirin Treatment Influences Platelet-Related Inflammatory Biomarkers in Healthy Individuals but Not in Acute Stroke Patients. *Thromb. Res.* **2011**, *128*, e73–e80.
47. Fujita, Y.; Mie, M.; Kobatake, E. Construction of Nanoscale Protein Particle Using Temperature-Sensitive Elastin-Like Peptide and Polyaspartic Acid Chain. *Biomaterials* **2009**, *30*, 3450–3457.
48. Prasad, R. Y.; Wallace, K.; Daniel, K. M.; Tennant, A. H.; Zucker, R. M.; Strickland, J.; Dreher, K.; Kligerman, A. D.; Blackman, C. F.; DeMarini, D. M. Effect of Treatment Media on the Agglomeration of Titanium Dioxide Nanoparticles: Impact on Genotoxicity, Cellular Interaction, and Cell Cycle. *ACS Nano* **2013**, *7*, 1929–1942.
49. Herd, H.; Daum, N.; Jones, A. T.; Huwer, H.; Ghandehari, H.; Leh, C. M. Nanoparticle Geometry and Surface Orientation Influence Mode of Cellular Uptake. *ACS Nano* **2013**, *7*, 1961–1973.
50. Barth, B. M.; Shanmugavelandy, S. S.; Kaiser, J. M.; McGovern, C.; Altnoğlu, E. I.; Haakenson, J. K.; Hengst, J. A.; Gilius, E. L.; Knupp, S. A.; Fox, T. E.; *et al.* Photoimmunonanotherapy Reveals an Anticancer Role for Sphingosine Kinase 2 and Dihydrosphingosine-1-Phosphate. *ACS Nano* **2013**, *7*, 2132–2144.
51. Stefanick, J. F.; Ashley, J. D.; Kiziltepe, T.; Bilgicer, B. A Systematic Analysis of Peptide Linker Length and Liposomal Polyethylene Glycol Coating on Cellular Uptake of Peptide-Targeted Liposomes. *ACS Nano* **2013**, *7*, 2935–2947.